Available online at www.sciencedirect.com
SCIENCE DIRECT
Polymer 46 (2005) 4465–4473
polymer
www.elsevier.com/locate/polymer

Interface morphology and phase separation in polymer-dispersed liquid crystal composites

Ryan S. Justice[a], Dale W. Schaefer[a,*], Richard A. Vaia[b], David W. Tomlin[c], Timothy J. Bunning[b]

[a]*University of Cincinnati, P.O. Box 210012, Cincinnati, OH 45221, USA*
[b]*Air Force Research Laboratory, Materials and Manufacturing Directorate, WPAFB, OH 45433, USA*
[c]*UES Incorporated, Dayton, OH 45432, USA*

Available online 17 March 2005

Abstract

It is widely appreciated that electro-optic activity in polymer-dispersed liquid crystals (PDLCs) depends on separation of the polymer and liquid crystal (LC) phases. Since the phase structure develops in a non-equilibrium system, the morphology of the LC domains depends on the details of the chemical and physical processes active during domain formation. The nature of the interface between the polymer and liquid crystal phases is of particular interest. This work discusses the two-phase morphology in an acrylate-based system that develops during polymerization-induced phase separation (PIPS). Using small-angle X-ray scattering (SAXS) and ultra-small-angle X-ray scattering (USAXS), we find that interfaces in PDLCs developed from an acrylate-based recipe are more disordered than generally appreciated. Information gained from SAXS and USAXS is compared to data from scanning electron microscopy (SEM) and transmission electron microscopy (TEM). To elucidate the apparent discrepancies between imaging and scattering, we investigated the effects of SEM sample preparation. We observe significant alteration of the interface morphology due to the leaching of the LC phase.

Keywords: Small-angle X-ray scattering; Interface morphology; PIPS

1. Introduction

Polymer-dispersed liquid crystals (PDLCs) are of technological importance for electro-optic applications such as privacy windows, electro-optic shutters, and large-area flat-panel displays [1–4]. PDLCs are prepared by pre-mixing a low-molar-mass liquid crystal (LC) solvent and a monomer into a uniform syrup. These mixtures are then cured, leading to phase separation of the LC and polymer phases. Ultimately, sequestered pockets of the LC phase are embedded in a polymer matrix. These pockets may or may not be spherical, depending upon the nature of the PDLC recipe.

In most cases, the two-phase morphology that results falls into one of two categories, (1) a 'Swiss cheese' morphology where spherical LC droplets are embedded in a polymer matrix, or (2) a 'reverse morphology' where a continuous LC phase is embedded in a polymer bead-like matrix [5,6]. In the latter case, the LC phase does not have droplet character. Controlling LC domain morphology is important since it modulates the electro-optical properties of the PDLC [7,8].

In this work, we concentrate on the two-phase morphology that develops in a crosslinked acrylate polymer system by polymerization induced phase separation (PIPS). Previous work shows that the 'reverse morphology' [1,3,4,6] develops in these systems. Early in the reaction, a high-molecular-weight polymer network phase-separates as spherical beads [6] that appear aggregated into a loose network with pores varying in size and shape [4]. As polymerization continues, the polymer network becomes more rigid and traps the LC domains within the polymer matrix. These features have been attributed to liquid–gel phase separation that occurs when gelation precedes phase separation [9]. This topic and its implications for the interface morphology will be discussed in more detail later in this work. The interesting feature of these PDLCs is that, although the LC domains are not spherical droplets, the sequestered volume of LC is sufficient such that a cast film can still be electro-optically active [10,11].

Considerable research has been devoted to improving the

* Corresponding author. Tel.: +1 513 556 5431; fax: +1 206 600 3191.
E-mail address: dale.schaefer@uc.edu (D.W. Schaefer).

0032-3861/$ - see front matter © 2005 Elsevier Ltd. All rights reserved.
doi:10.1016/j.polymer.2005.02.029

optical efficiency of acrylate-based PDLCs [5]. The specific recipe discussed in this work has been investigated extensively with regard to holographically cured PDLC films (H-PDLC) [1,7,11,12]. The recipe has been optimized to sequester nanoscale LC domains (<100 nm), thereby eliminating scattering problems associated with larger two-phase structures [3]. To ensure nanoscale domains, high-functionality monomers are used as the majority constituent in the pre-polymer syrup [12]. Nanometer domains are necessary to yield PDLCs with high transmission, high diffraction efficiency, and fast poling response [1]. Bunning et al. investigated the use of highly functional monomers and solubilizers to control LC domain growth and restrict droplets to nanometer dimensions [1,7]. Using a high functionality monomer ensures fast kinetics that trap small LC droplets in the polymer matrix. Further, solubilizers are often added to increase the homogeneity of the pre-polymer syrup and reduce the viscosity generated by the highly functional monomer [12]. The use of a solubilizer reduces the crosslink density of the polymer matrix by scavenging double bonds in the penta-acrylate during the free-radical reaction [1]. Issues related to polymerization chemistry will be reported elsewhere.

Throughout the literature, most of the emphasis has concerned the relationship between inherent LC properties (elastic constants, viscosity, dielectric anisotropy, birefringence) and the electro-optical properties of the two-phase structure (contrast ratios, switching speeds). However, the optical characteristics of PDLCs are also dependent on polymer architecture and the nature and rate of polymerization, which determine the spatially varying two-phase structure [3]. Almost no research focuses on the polymer structure or the interfaces that develop between the polymer and LC phases. The bulk of the reported results rely on electron microscopy to characterize morphology [1,4,13]. For the few cases where small-angle scattering (SAS) has been used [2,3], the information available in the scattering profiles was not fully exploited.

The focus of this work is the effect of LC loading on the interface morphology and phase separation of a photo-initiated, free-radical-polymerized penta-acrylate/LC system. We used the complementary information provided by scanning electron microscopy (SEM), transmission electron microscopy (TEM) and ultra-small angle X-ray scattering (USAXS) to characterize the nanoscale morphology on length scales from 10 Å to 1 μm. When the LC concentration is increased, we observe increased domain size by SEM and USAXS. Micrographs of the leached samples show the expected reverse morphology, with the size and smoothness of the polymer 'beads' increasing as LC concentration increases. The USAXS data, however, suggest that even at the highest LC loading, the polymer/LC interface is very rough, which seems inconsistent with the distinct interfacial surface observed by SEM. Transmission electron microscopy (TEM) images verify the presence of disorder observed with USAXS. We investigate the SEM sample preparation for possible explanations for the discrepancies between these two analysis techniques. Specifically, small-angle X-ray scattering (SAXS) shows sample preparation for SEM alters the interfaces between the polymer/LC phases. Through the use of USAXS and SAXS, we conclude (1) the interfaces between the polymer/LC phases are more disordered than generally acknowledged, and (2) the sample preparation for SEM compromises the interpretation of the imaging data.

2. Experimental

2.1. Materials

Pre-polymer syrups consisting of monomer dipentaerythritol penta-/hexa-acrylate (DPHPA, 38–88%), photoinitiator rose bengal (0.6%), co-initiator *n*-phenyl glycine (NPG, 1.5%), and homogenizer n-vinylpyrrolidinone (NVP, 10%) were mixed with varying concentrations of liquid crystal E7 (0, 10, 20, 30, 40, 50%). All percentages listed are weight percentages. All constituents were acquired from Aldrich except the rose bengal (Spectra Group) and the LC-E7 (EM Industries). The samples were mixed into 1 g syrups and cured as 1.5 mm thick films. It should be noted that a curing gradient could be present due to the thickness of these samples. The films were flood-cured by exposure to two 20 W halogen lamps (one on each side of the sample) for 20 min. The incident power on the samples was approximately 100 mW/cm^2. These five samples were characterized using both USAXS and SEM.

Four samples were prepared for SAXS analysis using the same constituents in the pre-polymer syrup and technique. The LC concentrations for these four samples were 0, 10, 35, and 50%. To simulate SEM preparation, the LC in these four samples was leached using methanol (MeOH) extraction. The samples were soaked in MeOH for several hours and dried under vacuum.

2.2. Characterization

X-ray scattering results from electron density contrast between constituents and provides information about geometry and three-dimensional arrangement of scattering objects. Scattering at small angles is sensitive to large-scale inhomogeneities in electron density. USAXS provides reliable information about real-space structures ranging in size from 1 nm to a few μm. Structural information is gained by measuring the scattered intensity, I, as a function of scattering vector, q, which is related to the scattering angle (θ) by

$$q = (4\pi/\lambda)\sin(\theta/2) \quad (1)$$

where λ is the wavelength of the radiation in the medium. In our system, the intensity is measured on an absolute scale

and is reported as the differential scattering cross-section per unit sample volume per steradian, $d\Sigma/(Vd\Omega)$. Note that q has the units of reciprocal length so scattering at a given q is sensitive to real space inhomogeneities on the scale q^{-1}.

The small-q region required for evaluation of large-scale morphology is not accessible with conventional small-angle X-ray scattering, therefore USAXS was implemented where scattering angles approach seconds of arc. The data were obtained at the UNICAT beam line at the Advanced Photon Source at Argonne National Laboratory. The Bonse–Hart USAXS camera at this facility covers the regime of 10^{-4} $\text{Å}^{-1} \leq q \leq 0.1$ Å^{-1}. For each sample, an air background was subtracted. The data were desmeared using routines provided by UNICAT. The incident wavelength was 1 Å.

In addition to USAXS, SAXS was used to obtain additional data in the q-range 0.01 $\text{Å}^{-1} < q < 0.2$ Å^{-1}, using 1.54 Å X-rays. SAXS data were obtained using the Molecular Metronics pin-hole SAXS camera at the Air Force Research Laboratory at Wright Patterson Air Force Base. For each sample, an air background was subtracted. The analysis of the radially averaged SAXS data was completed using the same techniques as will be described for the USAXS data.

Low-voltage, high-resolution SEM was performed using a Hitachi S5200-UHR operated at 5 kV. Samples were prepared for SEM by peeling the films from a glass substrate with a razor blade. The LC droplets were then removed by MeOH extraction, generating voids where the LC once resided. The samples were fractured in liquid nitrogen to yield a cross-section representative of the bulk morphology. The samples were mounted and coated with 2–3 nm of tungsten using a dual ion beam sputter coater (South Bay Technologies, Inc.) to minimize the artifacts caused by sample charging.

TEM analysis was conducted on a JEOL 100CX transmission electron microscope operating at 100 kV. The bulk samples were embedded in Spurr's resin and cured in an oven overnight. The embedded blocks were then trimmed and sectioned using a 45° diamond knife on a Reichert ultramicrotome. The 60 nm sections were collected on 400-mesh copper hex grids.

3. Results

3.1. SEM analysis

We obtained several SEM images at each of six LC concentrations—0, 10, 20, 30, 40, and 50% LC. The 0% LC image is shown for reference (Fig. 1(a)). For the 10 and 20% LC samples we see little indication of distinct polymer and LC phases. The images (Fig. 1(b) and (c)) show finger-like projections developing from the surface of the sample but with no consistency in geometry or size. As the LC concentration is increased to 30% (Fig. 1(d)), evidence of phase separation emerges. The polymer matrix begins to form bead-like structures. The small voids within the bead-like matrix are the fingerprint left by the removal of the LC phase. At 40% LC (Fig. 1(e)), the bead-like polymer moieties are more spherical and smooth, and the voids left by the leached LC phase are more prevalent. At 50% LC (Fig. 1(f)), the polymer beads are more distinct and smooth, and the volume occupied by the LC continues to increase monotonically with LC loading, suggesting that the void space was indeed occupied by LC. Although it is difficult to quantify through two-dimensional imaging, the LC and polymer phases seem to be winding together in a bicontinuous structure. The voids and beads are quite polydisperse in size, ranging from 800 to 1500 Å.

In summary, the SEM data consistently show the expected reverse morphology with phase separation occurring in samples with LC loadings of 30% or greater. Above 30%, interfaces appear distinct and smooth, although it must be realized that tungsten coating necessarily smoothes the interfaces on length scales below 20 Å. These results are consistent with SEM analysis reported by Vaia et al. [3].

3.2. USAXS data

Quite a different morphological picture emerges from the USAXS data (Fig. 2). The curves in Fig. 2 can be characterized by dividing the scattering profiles into four regimes—a power-law regime at low q, an exponential regime, a power-law following the exponential regime, and background scattering at high q. The power-law regime at low q represents scattering from moieties whose size is too large to be characterized in the q-range of USAXS. Scattering in this regime is attributed to the sample surface. The 'knee' (Guinier regime) in a particular scattering profile that occurs on a log–log plot at intermediate q-values is indicative of exponential decay in scattered intensity that corresponds to an average structural size according to Guinier's law in exponential form [14]

$$I(q) \approx G \exp\left(-\frac{q^2 R_G^2}{3}\right) \tag{2}$$

where G is a prefactor determined by the concentration and composition of the scatterers and R_G is the so-called Guinier radius. If the scatterer is uniform in scattering-length density, then R_G is defined by [14]

$$R_G^2 = \frac{1}{v}\int r^2 \sigma(r) dr \tag{3}$$

where v is the volume of the scatterer and $\sigma(r)$ is the shape function, equal to 1 within its volume and 0 without, and r is taken to be at the center of mass (of scattering length density). Therefore, R_G is defined as the root-mean-square distance of all the points in the scatterer from its center of mass (with each point weighted according to its scattering length density) [14]. For independent particles, R_G is the radius of gyration. The Guinier regime is often followed by

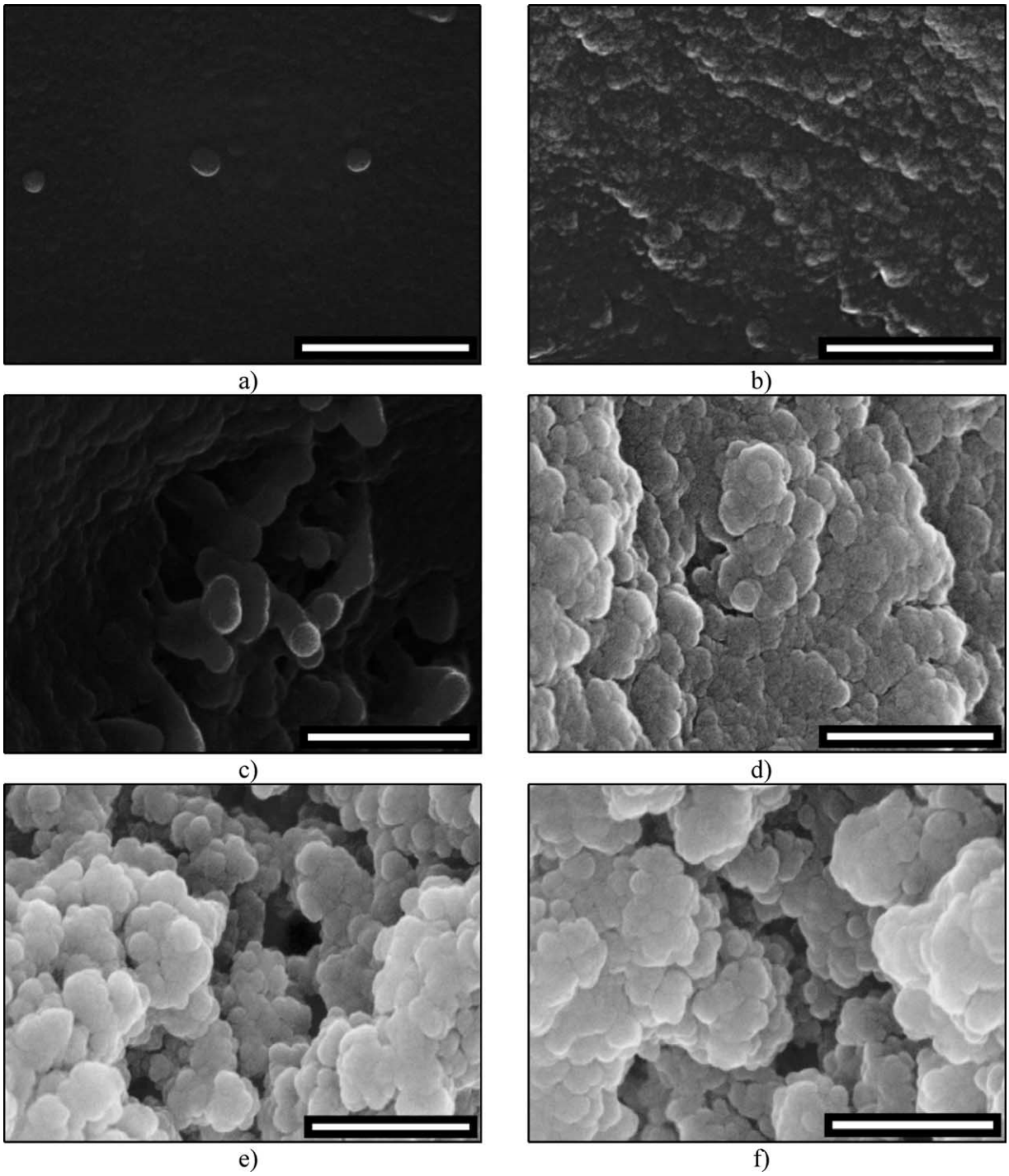

Fig. 1. SEM micrographs of (a) 0, (b) 10, (c) 20, (d) 30, (e) 40, (f) 50% LC samples. Scale bars correspond to 300 nm for (a)–(f).

a power-law regime that reflects the mass scaling with size of measurement following the equation

$$I \approx B\left(\frac{1}{q}\right)^{-P} \tag{4}$$

where P is the power-law exponent and B is the prefactor specific to the type of power-law scattering [15]. By combining the equations for the Guinier and associated power-law regime, we obtain the equation for one level of the scattering profile as:

$$I(q) \approx G\exp\left(-\frac{q^2R_G^2}{3}\right) + B\left(\frac{1}{q}\right)^{-P} \tag{5}$$

Eq. (5) is good for model fits (spheres, disks, rods) which display a single length scale and are rotationally and transitionally random. However, when the system does not

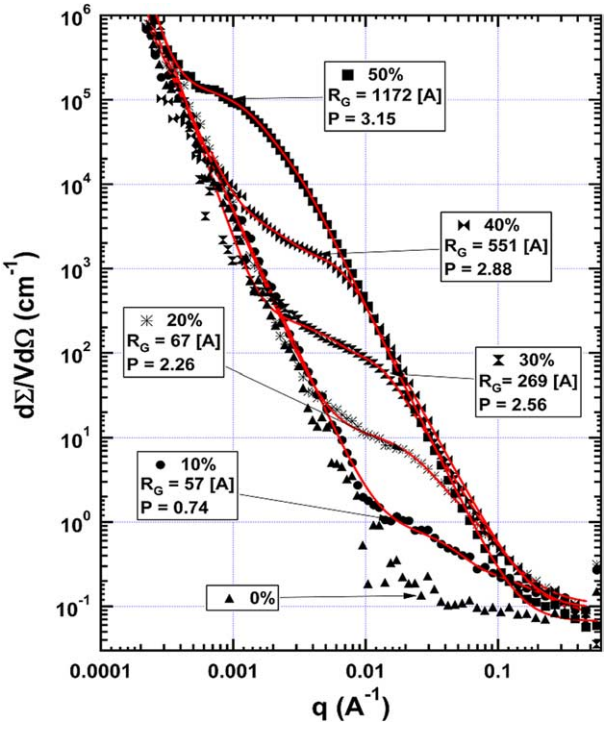

Fig. 2. USAXS data as a function of LC loading. Guinier radius (R_G) and power-law exponent (P) values are shown. As LC loading is increased, both the R_G and P values increase monotonically. However, even at the 50% LC concentration, the data suggest minimal indication of phase separation. The red lines represent the unified fits used to calculate the R_G and P values.

contain distinct particles or contains multiple size-scale structures (such is the case in our system and will explained later), Eq. (5) must be expanded [16].

For our system, where four distinct regimes are visible, Eq. (5) must be expanded into a multi-level fit, where the two regions of power-law scattering, the Guinier region, and the background scattering are considered in one 'unified fit'

$$I(q) \approx B_{\text{large}}\left(\frac{1}{q}\right)^{-P} + G\exp\left(-\frac{q^2R_G^2}{3}\right) + B\left(\frac{1}{q}\right)^{-P} + G_{\text{bkg}} \quad (6)$$

where B_{large} is the prefactor that corresponds to the power-law scattering that occurs at the lowest values of q, and G_{bkg} is a constant value generated by the background scattering. Eq. (6), however, is a simplified form of the unified equation. The exact fom of the unified equation can be found in reference 15 It should be noted that scattering accounted for in the first and last terms in Eq. (6) converge to the same values in all of the samples in Fig. 2 regardless of LC concentration, which includes the 0% LC sample. It is assumed that these contributions are not related to the domain structure characterized by the second and third terms of Eq. (6). Consequently, the first and last terms have no bearing on this analysis. The lines in Fig. 2 represent the fits generated using Eq. (6).

The characterization of phase separation can be obtained using the region of power-law scattering that occurs after the Guinier region. From the scattering curves, the value of P directly reveals the qualitative nature of the scattering entities and provides an immediate test for the presence of phase separated domains. For a smooth sharp interface, $P=4$, and the resulting equation $I \approx q^{-4}$ is Porod's law. A phase-separated system is expected to have smooth, sharp interfaces and therefore follow Porod's law. Deviations from Porod's law are attributed to interface roughness ($3<P<4$) or perhaps the complete absence of an interface ($P<3$). Bale and Schmidt showed that rough interfaces would deviate from the value $P=4$, but the scattering profile would still remain power-law for self-similar (or self-affine) fractal surfaces with $3<P<4$ [17]. The magnitude of P provides a measure of the roughness, which can be quantified through a surface fractal dimension, $D_s=6-P$, where $D_s=2$ corresponds to a smooth interface, and $D_s=3$ corresponds to a maximally rough interface. When P lies between 3 and 4, the surface area is not well defined since the interfacial area depends on the measurement length scale [18].

When the power-law exponent is <3, the system is referred to a mass fractal. Mass fractals are best thought of as irregular branched morphologies with no interface. A Gaussian chain, for example, is a mass fractal of dimension 2. A branched Gaussian chain has a fractal dimension between 2 and 3, the exact value depending on the details of the chain statistics. For mass fractals, the mass fractal dimension $D_m=P$ [18].

The data in Fig. 2 represent the USAXS scattering profiles for five concentrations of LC. Based on the previously explained analysis and P-values in Fig. 2, we see that these data disagree with the SEM data presented here and the literature by suggesting the samples containing concentrations 30%<LC<50% are mass fractals. In fact, only the 50% LC sample has a $P>3$, and at 3.15 it is only slightly above the threshold of surface fractal character. Consequently from these scattering data, without any further investigation, only the 50% sample could be considered to have a distinct interface between the polymer/LC phases, but the interface is much more disordered than what is postulated based on SEM images throughout the literature.

3.3. SAXS analysis

To further elucidate the discrepancies between the SEM and USAXS data, we investigated the effect of SEM sample preparation on the interface morphology using SAXS since SAXS was not available. Specifically, we measured the change in the scattering profiles caused by MeOH extraction. USAXS covers the range $0.01\ \text{Å}^{-1}<q<0.2\ \text{Å}^{-1}$, so P can be measured for all the samples.

Four LC concentrations were used for the leaching study—0, 10, 35, and 50%. The samples were weighed before and after MeOH treatment, and SAXS profiles were measured before and after MeOH extraction. Fig. 3

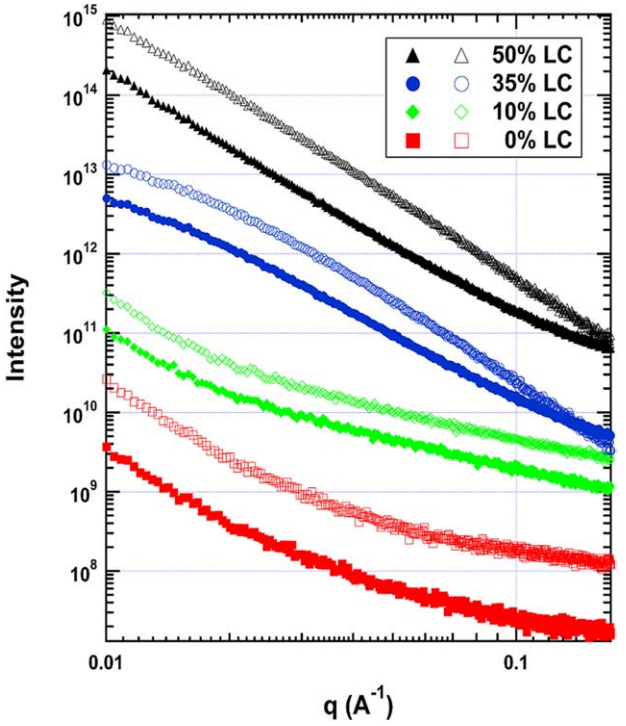

Fig. 3. SAXS profiles for 0, 10, 35, and 50% LC samples before and after leaching. Curves with closed markers indicate samples before MeOH extraction of the LC domains, and open markers indicate the LC domains have been leached leaving only the cured polymer. These data are not on an absolute scale, but the relative shift in intensity is accurate to about ±20%.

compares the scattering profiles of these samples. Although the data are not on an absolute scale, the relative change in intensity is accurate within ±20%. Similarly to the SEM data, these results are consistent to SAXS results reported by Vaia et al., although the interpretation of these data is somewhat different [3].

By visual inspection, one can see that the scattering profiles shift to higher intensity once the LC phase is removed (after MeOH extraction). The density of the cured polymer can be calculated from the ratio of the intensity for the leached and unleached sample using the formula:

$$\frac{I_{\text{leached}}}{I_0} = \frac{(\text{SLD}_{\text{polymer}})^2}{(\text{SLD}_{\text{polymer}} - \text{SLD}_{\text{matrix}})^2} = 3.33 \qquad (7)$$

where $\text{SLD}_{\text{polymer}} = 8.92 \times 10^{10}$ (cm/g)$\times\rho$, where ρ is the cured polymer density. The scattering length density (SLD) of the matrix is calculated to be 8.12×10^{10} cm^{-2} based on the composition of LC-E7 and a measured density of 0.9 g/cm^3. The average value of I_{leached}/I_0 for the four samples in Fig. 3 gives a ratio of 3.33. Therefore, by solving Eq. (7) for ρ, we obtain a value of 0.6 g/cm^3 for the cured polymer density. Given the assumptions and experimental errors involved, this value for the cured polymer density is consistent with the idea that the scattering is due to polymer-LC contrast.

The percentages by which the samples decreased in weight after MeOH extraction are: 0% = 4.6%, 10% = 3.4%, 35% = 38.8%, 50% = 52.4%. In the 0% LC case only small molecule additives and oligomers leach out. It is interesting to note that there is a large shift in intensity on leaching even when no liquid crystal is present. Also the shifted curves superimpose exactly below 35%, whereas there is a distinct change in shape above 35%.

For the 35 and 50% data, we see increases in the intensity in the data once the LC is removed from the system similar to the intensity shift observed at the lower concentrations. However, once the LC is removed from the samples, we see changes in the shape of the profiles for both the 35% and 50% samples. The slope of both curves decreases to −3.4 indicative of evolution from a rough interface to a smoother interface. Leaching seems to cause a collapse of the polymer molecules and smoothing of the interfaces. Nevertheless, the SAXS data still show the domain interfaces to be far from smooth even in the leached state (Fig. 4).

It seems clear that characterizing these flood-lit samples prior to SEM sample preparation as having distinct, smooth interfaces is not an accurate representation. The conclusion made from the USAXS and SAXS data is the morphology of these systems is altered by extraction of the LC phase. The highly phase separated systems suggested by the SEM is a consequence of leaching and sputter coating of the samples.

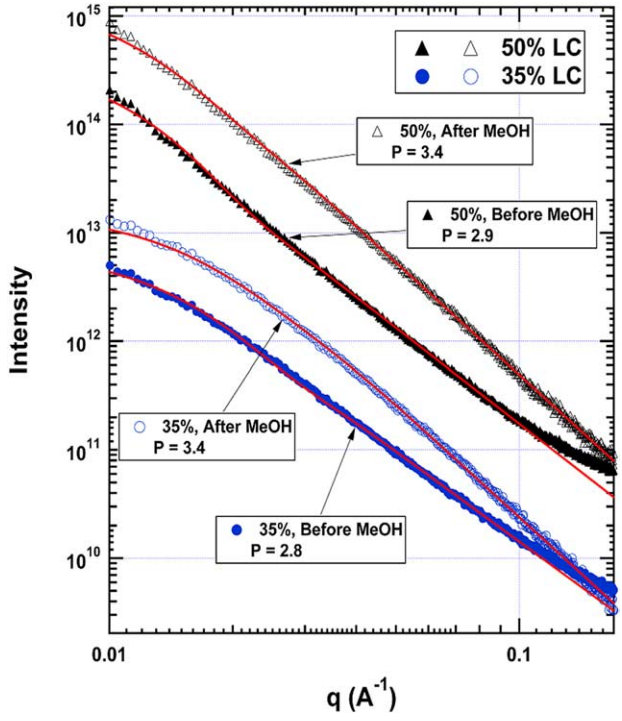

Fig. 4. Unified fit to the SAXS profiles before and after MeOH leaching for 35 and 50% loading. Closed markers represent samples before MeOH extraction, and open markers represent after MeOH extraction. Removal of the LC leads to substantial increases in the power-law exponent at both LC concentrations. These increases suggest the systems are becoming much more phase separated once the LC is removed via MeOH extraction. These data are not on an absolute scale. The red lines represent the unified fits used to calculate the P values.

4. Discussion

The results above show that LC domains are substantially more disordered than is generally recognized in the literature. The domains observed in this study do not qualify as droplets in the sense of quasi-spherical objects with sharp interfaces. The presence of disorder raises several issues. Why have these disordered phases not been identified previously? What is the origin of the disordered morphology? How does disorder affect electro-optic switching?

The reason disorder has not been recognized in previous studies is objects whose mass-fractal dimension, D_m, is larger than 2.0 appear as fully dense, solid objects when viewed in projection. In the present study, when we expect to see the onset of phase separation (LC concentrations $30\% < LC \leq 50\%$), we find $2.56 \leq D_m \leq 3.15$, so that all these systems will appear as uniformly dense droplets when viewed in projection. Only in the surface region, where the projected slice is thin, is there the possibility of observing disorder.

Fig. 5 shows a TEM image of a system where we expect $D_m \cong 2.9$ based on USAXS. As expected, the LC domains (light areas) appear as non-spherical, disordered domains. Moreover, the edges of the projected domains are quite irregular. Although one might suspect the presence of disorder based on the irregularity of the LC domains, it is impossible to tell if the domains are fully dense ($D_m = 3$), uniformly dense with smooth interfaces ($D_m = 3$), uniformly dense with rough interfaces ($D_m = 3$), or mass fractals with $2 < D_m < 3$.

Many imaging studies of LC composites are based on optical microscopy. Of necessity, the domains must be of the order of 1 μm to be observed. It is not surprising that conditions that lead to micron-sized domains produce true droplets. Nevertheless, evidence exists for disorder even in the optical images. For example, Serbutoviez et al. explained that at LC loadings below 60%, domains 'are so small that it is impossible to say whether they are spherical or non-spherical' [19]. These authors also note that the LC domains are more deformed at lower LC loading and that 'a spaghetti-like structure develops toward the end of the process in most cases' [19].

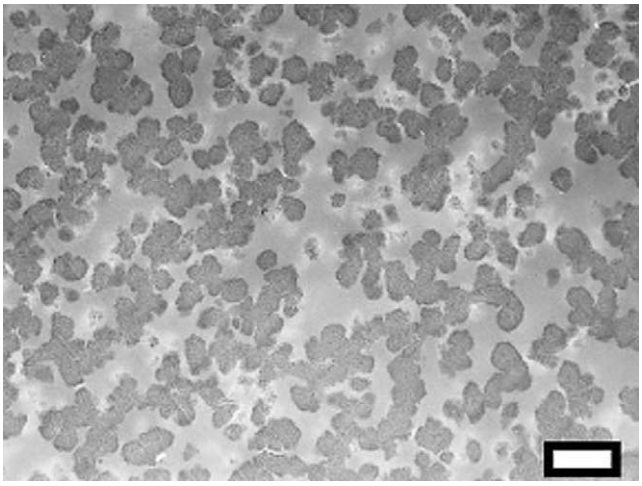

Fig. 5. TEM at 10 K magnification of 40% LC sample cured at 48 mW/cm^2. The expected P-value for sample at this concentration, as determined from the data in Fig. 2, is $P = 2.9$. The LC domains (light areas) in this image appear disordered with irregular edges. From this two-dimensional image, it is difficult to draw any conclusions about the fractal nature of the LC. The scale bar corresponds to 100 nm.

Amundson, vanBlaaderen and Wiltzius [20], on the other hand, observe filamentary polymeric domains by confocal microscopy within the LC domains. Although the length scale of the filamentous polymers is much larger in these images compared to our materials, the filamentary nature is consistent with the type of disorder we find at low LC loading. In summary, the existing literature supports the idea that submicron domains are disordered. Our work corroborates these observations and provides detailed information on the nature of the domains.

The origin of disorder is also implicit in the literature. For example, Boots et al. discuss the phase behavior of LC-acrylate systems based on a Flory–Huggins model of a polymer network (gel) polymerizing in a mixture of LC and monomer [9]. This model predicts the phase behavior based on the degree of polymerization of the polymer. The assumption is that the LC-rich phase is pure LC, whereas the polymer-rich phase is a mixture. Based on this theory and experimental observations, these authors conclude the gelation of the polymer network occurs before phase separation into two distinct domains [9].

Although the Flory–Huggins approach does not predict phase morphology, it is easy to rationalize the presence of disorder in the domain morphology. Disorder arises from topological fluctuations in the polymer network at the time of phase separation. Since the system is crosslinked, phase separation requires exclusion of the LC from the polymer. The network is rapidly becoming rigid, however, which limits domain coalescence. The kinetically favorable path to phase separation is the formation of submicron pockets of LC within the polymer network. The LC collects in regions of low crosslink density. It is reasonable that the resulting LC domains have rough surfaces due to the native topology fluctuations in the precursor gel. The polymer matrix does not collapse uniformly as it would for liquid–liquid phase separation. Rather, the network collapses irregularly, dictated by random fluctuations in the elastic energy of the gel. Highly crosslinked regions collapse, while loosely crosslinked regions stretch to accommodate the LC phase. Although this qualitative argument does not demand that the interfaces be fractally rough, it is reasonable to assume that topological fluctuations would have fractal character since, to first approximation, gelation is simple percolation.

Boots et al. offer an alternative argument that could account for the fractal nature of the LC domains [9]. The initial phase separation event leads to a pure LC phase and a polymer-LC mixed phase. Further polymerization leads to secondary phase separation in the polymer-rich phase

leading to smaller pure LC domains embedded in a matrix that is now richer in polymer. Iteration of this cycle leads to pure, ever-smaller LC domains whose size may well be power-law distributed leading to scattering profiles that are indistinguishable from quasi-monodisperse domains with rough surfaces. This scheme can account for our data at high LC loading (35%), but it is not clear that it can account for the low-LC systems where the magnitude of the power-law exponent is less than three. Therefore, we favor the idea that topological fluctuations lead to fractal domain structures.

If the domain morphology is controlled by topological fluctuations, what is the significance of the crossover from mass-fractal character for LC $<$ 35% to surface fractal character for LC $>$ 35%? The simplest explanation is that the low-LC systems are not phase separated and should be thought of as a randomly branched polymer swollen with LC and residual monomer. The LC and other small molecules (including monomer and oligomers) serve as the milieu in which the growing polymer develops. Since the polymer-LC solution does not show electro-optic activity, the absence of switching at low LC loading is consistent with the polymer solution explanation. Alternatively, at low LC, these domains may simply be too small to show bulk behavior.

If the path to phase separation is as described above, the LC phase is pure and will show electro-optic behavior if the LC concentration is sufficiently large. The idea of a fractally rough interface is not the same as a graded interface, which would show local slopes in the scattering profiles more negative than -4. The interfaces we observe remain sharp even though they are not smooth. Although fractal roughness may necessitate larger domains to exhibit an electro-optic effect, such disorder does not preclude optical activity.

5. Conclusions

This study suggests that high intensity, flood-lit curing of a specific acrylate-based recipe produces the so-called reverse morphology, which is consistent with previous findings [3]. At low-LC concentrations, the systems are not phase separated and should be thought of as a randomly branched polymer swollen with LC and residual monomer that will not electro-optically switch. As the LC concentration is increased to a sufficiently large percentage such that phase separation is induced (30–35% LC), the systems phase separate into distinct polymer and LC phases with a sharp, but fractally rough interface. Although fractal roughness may necessitate larger domains for electro-optic effect, such disorder does not preclude optical activity. Although the USAXS data seem inconsistent with the conventional wisdom regarding PDLCs, we show that scattering profiles are consistent with the literature while providing more detailed information on the submicron structures.

Although this study cannot be casually generalized to other composite systems formed by PIPS, the observations should evoke a degree of caution regarding the interpretation of SEM images. The SAXS analysis shows that MeOH extraction of the LC phase from these composites alters their morphology. The domain collapse that occurs when the LC phase is removed should be taken into account in future SEM analysis of PDLC systems.

Acknowledgements

Dale Schaefer was introduced to PIPS by the work of James E. Mark. Mark's goal was in situ generation of reinforcing fillers in silicone rubbers. In a long-term collaboration that developed at Sandia National Laboratories where Mark was a summer visiting faculty, we initiated a fruitful investigation of the nature of phase separation in silicone elastomers using SAXS. Many of the ideas in this paper on PDLCs stem from those collaborations.

We thank Pete Jemian and Jan Ilavsky for assistance in collection of the USAXS data. The UNICAT facility at the Advanced Photon Source (APS) is supported by the University of Illinois at Urbana-Champaign, Materials Research Laboratory (U.S. Department of Energy, the State of Illinois-IBHE-HECA, and the National Science Foundation), the Oak Ridge National Laboratory (U.S. DOE under contract with UT Battelle LLC), the National Institute of Standards and Technology (U.S. Department of Commerce) and UOP LLC. The APS is supported by the U.S. Department of Energy, Basic Energy Sciences, Office of Science under contract No. W-31-109-ENG-38. Work at the University of Cincinnati was supported by the Air Force Research Laboratory through the Anteon Corporation.

We also thank Lalgudi Natarajan (Science Applications International Corporation, Dayton, OH) and Jay Klosterman (Air Force Research Laboratory, Materials and Manufacturing Directorate, WPAFB, OH) for the preparation of the polymer/LC samples discussed in this work.

References

[1] Bunning TJ, Natarajan LV, Tondiglia VP, Dougherty G, Sutherland RL. J Polym Sci, Part B-Polym Phys 1997;35:2825–33.
[2] Leclercq L, Maschke U, Ewen B, Coqueret X, Mechernene L, Benmouna M. Liq Cryst 1999;26:415–25.
[3] Vaia RA, Tomlin DW, Schulte MD, Bunning TJ. Polymer 2001;42:1055–65.
[4] Rajaram CV, Hudson SD, Chien LC. Chem Mater 1996;8:2451–60.
[5] Drzaic PS. Liquid crystal dispersions. Singapore: World Scientific; 1995.
[6] Yamagishi FG, Miller LJ, Van Ast CI. Proc SPIE 1989;1080:24–31.
[7] Pogue RT, Natarajan LV, Siwecki SA, Tondiglia VP, Sutherland RL, Bunning TJ. Polymer 2000;41:733–41.
[8] Natarajan LV, Shepherd CK, Brandelik DM, Sutherland RL, Chandra S, Tondiglia VP, et al. Chem Mater 2003;15:2477–84.

[9] Boots HMJ, Kloosterboer JG, Serbutoviez C, Touwslager FJ. Macromolecules 1996;29:7683–9.
[10] Natarajan LV, Sutherland RL, Tondiglia VP, Bunning TJ, Adams WW. J Non-linear Opt Phys Mater 1996;5:89–98.
[11] Bunning TJ, Natarajan LV, Tondiglia VP, Sutherland RL. Annu Rev Mater Sci 2000;30:83–115.
[12] Klosterman J, Natarajan LV, Tondiglia V, Sutherland RL, White T, Guymon CA, et al. Polymer 2004;45:7213–8.
[13] Rajaram CV, Huson SD, Chien LC. Chem Mater 1995;7:2300–8.
[14] Roe RJ. Methods of X-ray and neutron scattering in polymer science. New York: Oxford University Press; 2000.
[15] Beaucage G. J Appl Crystallogr 1996;29:134–46.
[16] Beaucage G, Schaefer DW. J Non-Cryst Solids 1994;172:797–805.
[17] Bale HD, Schmidt PW. Phys Rev Lett 1984;53:596–9.
[18] Schaefer DW, Beaucage G, Loy DA, Shea KJ, Lin JS. Chem Mater 2004;16:1402–10.
[19] Serbutoviez C, Kloosterboer JG, Boots HMJ, Touwslager FJ. Macromolecules 1996;29:7690–8.
[20] Amundson K, vanBlaaderen A, Wiltzius P. Phys Rev E 1997;55: 1646–54.